



Cite this: *Biomater. Sci.*, 2021, **9**, 7124

# A multifunctional green antibacterial rapid hemostasis composite wound dressing for wound healing†

Wencheng Liang,<sup>a,b</sup> Qiaohui Lu,<sup>c</sup> Fan Yu,<sup>d</sup> Junyong Zhang,<sup>a</sup> Chuang Xiao,<sup>a</sup> Xiaoming Dou,<sup>b</sup> Yan Zhou,<sup>c</sup> Xiumei Mo,<sup>d</sup> Jun Li<sup>d</sup> \*<sup>e</sup> and Meidong Lang<sup>d</sup> \*<sup>a</sup>

Rapid hemostasis and antibacterial properties are essential for novel wound dressings to promote wound healing. In particular, timely and rapid hemostasis could be of benefit to reduce the mortality caused by excessive bleeding loss. Herein, we present a novel strategy of combining electrospinning technology with post-modification technology to prepare a multifunctional wound dressing, cellulose diacetate-based composite wound dressing (CDCE), with rapid hemostasis and antibacterial activity. It is interesting that the CDCE wound dressing had superhydrophilicity, high water absorption, and strong absorbing capacity, which could eliminate the exudate around the wound in a timely manner and further promote rapid hemostasis. Additionally, its excellent antibacterial properties could inhibit severe infection in the wound and accelerate wound healing. Based on these advantages, the novel CDCE wound dressing could promote wound contraction and further accelerate wound healing compared with the common traditional wound dressing gauze. Taken together, the multifunctional CDCE wound dressing has high potential for clinical application in the future.

Received 30th July 2021,  
Accepted 6th September 2021

DOI: 10.1039/d1bm01185e

rsc.li/biomaterials-science

## 1. Introduction

Wound healing is a complex process that can be divided into four phases: hemostasis, inflammation, proliferation and remodeling of the wound structure.<sup>1,2</sup> During the wound healing process, excessive bleeding and wound infection cause higher mortality.<sup>3</sup> Thus, rapid hemostasis is one of the efficient strategies to reduce mortality.<sup>2,4</sup> In addition, the wound bed, a nutrient-rich micro-environment, could increase

the risk of wound infection and hinder wound healing.<sup>5,6</sup> Therefore, wound dressings with rapid hemostasis and excellent antibacterial properties are important for accelerating wound healing and promoting damaged tissue regeneration. In comparison with traditional wound dressings, novel wound dressings should be multifunctional for promoting wound healing, including rapid hemostasis, antibacterial activity, hemocompatibility, biocompatibility, and acceleration of damaged tissue regeneration.<sup>7</sup> In recent decades, various antibacterial agents have been developed continuously in the field of wound dressings, such as antibiotics, metals or metal oxides and cationic antibacterial agents.<sup>8–10</sup> However, more safe antibacterial agents have attracted much attention, such as natural polypeptides.<sup>11,12</sup> In comparison with antibiotics and metal-based antibacterial agents, polypeptides possess excellent biocompatibility and are eco-friendly. In particular, epsilon poly-lysine ( $\epsilon$ -PL) has a broad-spectrum antibacterial ability. The degradation products of  $\epsilon$ -PL are not significantly toxic to the body.<sup>13,14</sup>

Polysaccharides and polysaccharide derivatives have attracted much attention in the field of wound dressings owing to their excellent biocompatibility and biodegradability.<sup>15</sup> In particular, cellulose has been selected as one of the important renewable materials due to its abundant resources, low-cost, biodegradability and biocompatibility. However, cellulose has no intrinsic antibacterial ability or solubility in organic solutions, which hinders its application as a wound

<sup>a</sup>Shanghai Key Laboratory of Advanced Polymeric Materials, Key Laboratory for Ultrafine Materials of Ministry of Education, School of Materials Science and Engineering, East China University of Science and Technology, 130 Meilong Road, Shanghai 200237, PR China. E-mail: mlang@ecust.edu.cn

<sup>b</sup>Center of Photonics & Bio-Medical Diagnosis, School of science, East China University of Science and Technology, 130 Meilong Road, Shanghai 200237, PR China

<sup>c</sup>State Key Laboratory of Bioreactor Engineering, School of biotechnology, East China University of Science and Technology, 130 Meilong Road, Shanghai 200237, PR China

<sup>d</sup>State Key Laboratory for Modification of Chemical Fibers and Polymer Materials, College of Chemistry, Chemical Engineering and Biotechnology, Donghua University, Shanghai 201620, PR China

<sup>e</sup>Department of Orthopedics, Shanghai Tenth People's Hospital Affiliated to Tongji University, 301 Yanchang Road, Shanghai 200072, PR China.  
E-mail: lijunspine@163.com

† Electronic supplementary information (ESI) available: Preparation of the RBC and rich platelet suspension solution; SEM; photographs of the hemolysis rate, BCI, and RBC attachment. See DOI: 10.1039/d1bm01185e

dressing alone.<sup>15,16</sup> To address these challenges, many cellulose derivatives have been developed in recent decades, such as cellulose diacetate (CDA).<sup>15,17</sup> Interestingly, CDA not only displays the advantages of cellulose, but also has excellent solubility and spinnability.<sup>18</sup>

Electrospinning technology has many advantages, such as facial preparation of nanofibers, mimicking the extracellular matrix (ECM) structure, and high porosity.<sup>19</sup> However, electrospun membranes with small pore sizes and low thickness have limited applications in some special biomaterial fields.<sup>20</sup> Thus, it is necessary to fabricate a three-dimensional (3D) structure with the desired shape and a suitable pore-size in the wound dressing field. Post-modification is one of the efficient strategies to prepare multifunctional 3D wound dressings by electrospinning.<sup>21–23</sup> Briefly, electrospun nanofibers are sheared into short fibers by mechanical shearing equipment, and then used to fabricate a 3D wound dressing *via* a freeze-drying method.<sup>21</sup>

In this work, we propose a novel strategy to fabricate a low cost and easy to use multifunctional CDCE wound dressing with a 3D structure, superhydrophilicity, rapid and effective hemostasis, excellent antibacterial activity, and effective wound healing through combining electrospinning and post-modification technology. Benefitted from the electrospinning and post-modification, the CDCE wound dressing had high porosity and superhydrophilic properties, which could improve water absorption, give strong absorbing capacity, allow rapid hemostasis, and provide a suitable micro-environment. Besides, its antibacterial properties could inhibit excessive wound infection and promote wound healing. Based on these advantages, we believe that the novel CDCE wound dressing has high potential for clinical applications in the future.

## 2. Results and discussion

### 2.1 Wound dressing structure characterization

The cross-linked CDA wound dressings were co-deposited with CMC and DA in Tris-HCl buffer solution and the as-prepared wound dressings (CDA/CMC@PDA) were obtained. Furthermore,  $\epsilon$ -PL was grafted into the CDA/CMC@PDA wound dressing. The FT-IR spectrum of the wound dressing is shown in Fig. 1a. In comparison with the CDA wound dressing,<sup>18,24</sup> the absorbance peaks of the CDA/CMC@PDA wound dressing were stronger at  $\sim 3475\text{ cm}^{-1}$ ,  $2958\text{ cm}^{-1}$ ,  $\sim 2850\text{ cm}^{-1}$ ,  $1750\text{ cm}^{-1}$  and  $1437\text{ cm}^{-1}$  owing to CMC and DA being introduced into the CDA wound dressing.<sup>25,26</sup> After being modified with  $\epsilon$ -PL, the peak of reactive hydrogen groups was moved to  $\sim 3442\text{ cm}^{-1}$  owing to a strong hydrogen bond. Besides, the absorbance peak of the amide at  $1630\text{ cm}^{-1}$  was enhanced due to the amide reaction between  $-\text{NH}_2$  and  $-\text{COOH}$ .<sup>27</sup> As abovementioned, the CDCE wound dressing was successfully prepared.

The morphology, WVRT, porosity and hydrophilicity are vital properties for wound dressings. A multifunctional wound dressing with pore connectivity, high porosity and superhydrophilicity could be of benefit to quickly eliminate wound

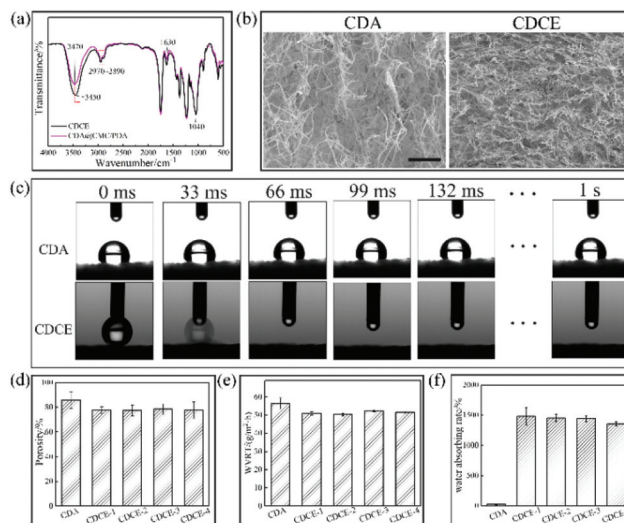


**Fig. 1** The structural characterization of the wound dressing. (a) The FT-IR of the wound dressing. (b) The SEM of the wound dressing (scale bar: 100  $\mu\text{m}$ ). (c) The water contact angle of the wound dressing at different time points. (d) The porosity of the wound dressing. (e) The water vapor transmission rate (WVRT) of the wound dressing. (f) The water absorbing rate of the wound dressing (10 s).

exudate, which could provide a balanced moist micro-environment to promote wound healing.<sup>28</sup> The SEM images (Fig. 1b) clearly show many connected and large-size pores in the wound dressing, which are caused by ice-crystals in the freeze-drying process.<sup>29</sup> In addition, the CDCE wound dressing porosity (Fig. 1d) was nearly 80%. The WVRT (Fig. 1e) of the CDCE wound dressing was lower than that of the CDA wound dressing, but the WVRT of the CDCE wound dressing was higher than  $50\text{ g m}^{-2}\text{ h}^{-1}$ , which indicated that the CDCE wound dressing could efficiently promote gas exchange and provide a moist micro-environment to promote wound healing.<sup>30</sup> The water contact angle (Fig. 1c) of the wound dressing showed that the CDCE wound dressing could completely absorb water within 66 ms, which indicated that the CDCE wound dressing had high water absorption and superhydrophilicity. Besides, the water absorbing capacity (Fig. 1f) of the CDCE wound dressing was up to 1300% within 10 s. However, the absorbing capacity of the CDA wound dressing was as low as 22% within the same time. As abovementioned, the CDCE wound dressing not only had high water absorption, but also strong water absorbing capacity. Thus, the CDCE wound dressing could eliminate wound exudate and maintain a balanced moist micro-environment. Additionally, high water-absorption, strong water capacity and high porosity could be of benefit to improve the concentration of coagulation components in the wound bed, and further promote the formation of blood clots and accelerate hemostasis.<sup>31</sup>

### 2.2 *In vitro* antibacterial assay

Bacterial infection is one of the major reasons that inhibits the wound healing process. Thus, it is important for wound dressings to have excellent antibacterial ability to prevent an exces-

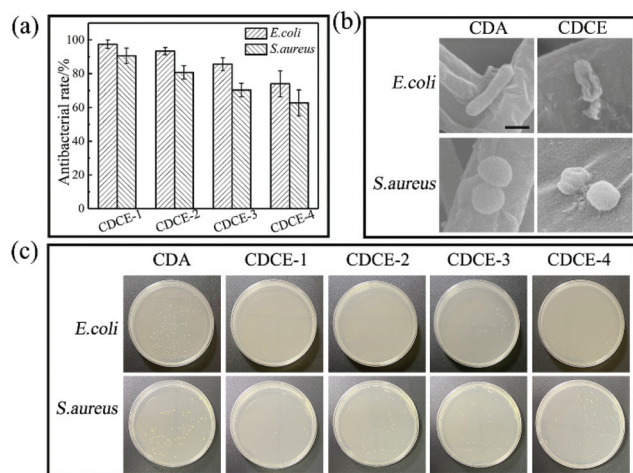


**Fig. 2** Antibacterial activity of the wound dressings against *E. coli* and *S. aureus*. (a) The antibacterial rate of the wound dressings. (b) Micrographs of *E. coli* and *S. aureus* (scale bar: 1  $\mu\text{m}$ ). (c) Photographs of the agar plates.

sive bacterial inflammatory response.<sup>32,33</sup> The antibacterial rate (Fig. 2a) of the CDCE wound dressing against *E. coli* was above 70%, and that against *S. aureus* was above 60%. In particular, the antibacterial rate of the CDCE-1–2 wound dressings was above 80% for *E. coli* and *S. aureus*, which indicated that the CDCE-1–2 wound dressings had excellent antibacterial ability. Through the bacterial colonies on the agar plates (Fig. 2c), it could be observed that the number of bacterial colonies after being co-cultured with the CDCE wound dressing was lower than that with the CDA wound dressing. Besides, the micrographs showed that the bacterial membranes of *E. coli* and *S. aureus* (Fig. 2b) were intrinsically complete and smooth. Briefly, the morphology of normal *E. coli* and *S. aureus* is a rod and spherical shape, respectively. However, the bacterial morphology was changed significantly after being co-cultured with the CDCE wound dressing. The *E. coli* and *S. aureus* membranes were wrinkled and displayed an irregular membrane morphology. Even some sheet-like structures of *E. coli* could be observed on the membrane surface. The SEM morphology indicated that the antibacterial mechanism of the CDCE wound dressing was to destroy the bacterial membrane through contact with rich-cationic polymers, owing to the cationic peptide of  $\epsilon$ -PL changing the zeta potential of the bacterial membrane and destroying the membrane structure further.<sup>14</sup> Taken together, the CDCE wound dressing had excellent antibacterial ability, which could prevent wound infection from bacteria. However, the CDCE-4 wound dressing was not studied further owing to its low antibacterial capacity.

### 2.3 *In vitro* blood assay

Hemocompatibility is one of the vital indices for evaluating wound dressings. The international permeation level of a hemocompatible biomaterial is below 5%.<sup>34</sup> In this work, the hemolysis rate of all wound dressings was far below 5%.

Briefly, that of the CDA wound dressing was 1.5%. That of the CDCE wound dressing was below 1%, which indicated that the CDCE wound dressing had excellent hemocompatibility. Hemostasis is the first step in the wound healing process for acute trauma.<sup>35</sup> Therefore, rapid hemostasis wound dressings could reduce blood loss and mortality. The BCI (Fig. 3b) of the CDCE wound dressing was nearly 20%. Meanwhile, the BCI of the CDA wound dressing was above 40%, which indicated that the CDCE wound dressing had higher blood clotting capacity than the CDA wound dressing.<sup>31</sup> In the hemostasis process, RBCs and platelets gathered on the wound bed are essential for accelerating hemostasis. In comparison with the CDA wound dressing, the CDCE wound dressing had a higher RBC attachment rate within 1 min. The RBC attachment rate of the CDCE wound dressing was nearly 80%, while that of the CDA wound dressing was as low as 22%. The micrographs of the RBCs and platelets (Fig. 3d) also indicated more RBC and platelet adhesion and/or aggregation on the wound dressing surface. This was caused by electrostatic interactions between the RBCs/platelets and wound dressing.<sup>31</sup> The CDCE wound dressing surface has numerous positive charges. Conversely, the RBC membrane and platelets show a weak negative charge, which was helpful for the adhesion and aggregation of red blood cells and platelets on the surface of the CDCE wound dressing.<sup>36</sup> Platelets could rapidly accumulate in the wound bed and induce more platelet aggregation on the wound bed, which could help to form blood clots and reduce blood loss.<sup>37</sup> Based on these properties, the CDCE wound dressing could achieve rapid hemostasis.

### 2.4 *In vivo* hemostasis assay

To mimic the hemostatic effect of the CDCE wound dressing in clinical applications, the liver hemostasis assessment of the wound dressings was carried out.<sup>38,39</sup> The hemostasis results

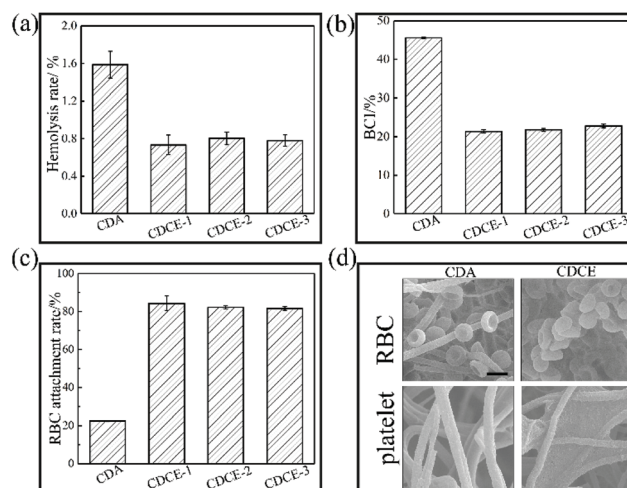


**Fig. 3** The blood assessment of the wound dressings *in vitro*. (a) The hemolysis rate of the wound dressings. (b) The BCI of the wound dressings. (c) The RBC attachment rate of the wound dressings (1 min). (d) Micrographs of the RBC and platelet morphology (scale bar: 5  $\mu\text{m}$ ).

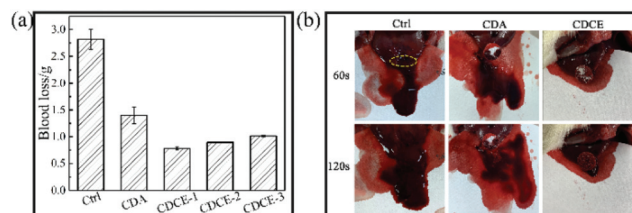


**Fig. 4** Hemostasis assessment of the wound dressings *in vivo*. (a) Blood loss from a liver wound. (b) Photographs of the hemostatic ability of the CDCE wound dressing (yellow circle: bleeding liver wound).

are shown in Fig. 4. The amount of blood loss of the control group (Ctrl) was high at 2.8 g within 2 min. In comparison with the control, the amount of blood loss with the CDA wound dressing was decreased to 1.4 g within 2 min. It was interesting that the amount of blood loss with the CDCE wound dressing was less than 1 g at the same time. In addition, the amount of blood loss with the CDCE wound dressing decreased as the amount of  $\epsilon$ -PL increased. The hemostatic effect of the CDCE wound dressing is shown in Fig. 4b; a large amount of blood was absorbed by the filter paper in the control, followed by the CDA wound dressing and the least was observed with the CDCE wound dressing. Thus, the CDCE wound dressing had more excellent rapid hemostasis capacity, which could be of benefit to reduce mortality caused by excessive blood loss.

### 2.5 *In vitro* cytocompatibility assay

The cell attachment rate (Fig. 5a) indicated that the CDCE wound dressing could promote cell attachment owing to the DA introduced into the wound dressing surface. According to a previous study, catechol groups can increase cell attachment and be of benefit to cellular behaviors.<sup>20</sup> Within 12 h, the cell attachment rate of the CDCE wound dressing was above 45%, but the cell attachment rate of CDA was less than 40%. The cytotoxicity of the wound dressings was evaluated by CCK-8 assays on the 2<sup>nd</sup>, 4<sup>th</sup> and 6<sup>th</sup> day. The results of cell viability are shown in Fig. 5b. In comparison with the CDA wound dressing, the CDCE wound dressing showed higher cell viability. However, there is no significant difference among the CDCE wound dressings in terms of the cell viability. Briefly, the cell viability of the CDCE wound dressing was up to 125%–129% on the 2<sup>nd</sup> day. With extension of the co-cultured time, the cell viability was up to 134%–143% on the 4<sup>th</sup> day and stabilized on the 6<sup>th</sup> day. The cell morphology was observed by SEM and laser confocal microscope. The SEM images showed that the MSCs (Fig. 5c) on the CDA wound dressing surface tended to gather-together along the fibers. However, the MSCs on the CDCE wound dressing tended to be flat and less gathered-together, which might be caused by the greater hydrophilicity of the CDCE wound dressing. The confocal images showed that the MSCs (Fig. 5d) were closely connected on the surface with a spindle-like morphology and distributed on the surface of the wound dressing. Briefly, all of the merged confocal images were mainly green with less red fluorescence, which

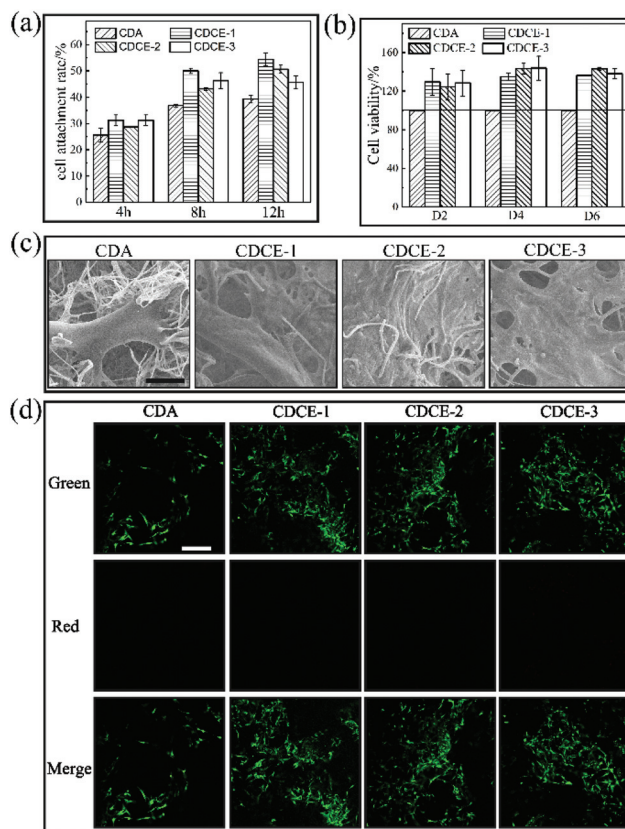


**Fig. 5** The cytocompatibility assessment of the wound dressings *in vitro*. (a) The cell attachment rate of the wound dressings at different time points. (b) The cell viability of the wound dressings co-cultured with MSCs on the 2<sup>nd</sup>, 4<sup>th</sup> and 6<sup>th</sup> day. (c) Micrographs of the MSCs on the wound dressings (scale bar: 40  $\mu$ m). (d) Confocal images of MSCs co-cultured with the wound dressings on the 6<sup>th</sup> day. The green and red fluorescence are living and dead MSCs, respectively (scale bar: 200  $\mu$ m).

indicated that the cells were alive with normal metabolism.<sup>40</sup> Besides, more cells were distributed on the CDCE wound dressing compared with the CDA wound dressing. In addition, the MSCs co-cultured with the CDCE wound dressing presented higher cytoskeleton elongation and cell spreading area than those on the CDA wound dressing. Thus, the CDCE wound dressing was nontoxic and could promote cell proliferation.

### 2.6 *In vivo* wound assay

To further study the wound healing effect of the CDCE wound dressing *in vivo*, a cutaneous wound model was created and treated with the various wound dressings.<sup>41</sup> The wound healing results *in vivo* are shown in Fig. 6. The wound contraction rate of the wounds treated with the various wound dressings and gauze are shown in Fig. 6a. In comparison with the gauze and CDA wound dressing, the CDCE-1–2 wound dressings could significantly promote wound contraction, and the wound contraction rate was nearly 100% on the 14<sup>th</sup> day, which was consistent with the photographs of wound healing (Fig. 6b). On the 7<sup>th</sup> day, in comparison with the CDA wound

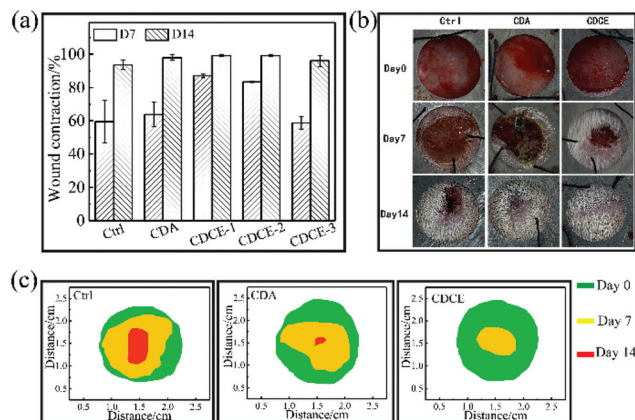


**Fig. 6** The wound healing assay *in vivo*. (a) The contraction of the wounds treated with different wound dressings. (b) The photographs of the wound healing on the 0<sup>th</sup>, 7<sup>th</sup> and 14<sup>th</sup> day. (c) Schematic diagram of the wound healing on the 0<sup>th</sup>, 7<sup>th</sup> and 14<sup>th</sup> day.

dressing and gauze, the wound area treated with the CDCE wound dressing was smaller, especially that treated with the CDCE-1–2 wound dressings. In addition, less wound exudate was observed on the wound bed treated with the CDCE wound dressing, while significant tissue exudate aggregation could be observed in the gauze group and CDA wound dressing group. This is owing to the CDCE wound dressing having higher water absorption and water absorbing capacity, while those of the gauze and CDA wound dressing were poor. Excessive accumulation of wound exudate on the wound bed could promote an excessive inflammatory response and inhibit wound healing.<sup>33,42</sup> Therefore, the CDCE-1–2 wound dressings could promote wound closure and accelerate wound healing.

## 2.7 Histological analysis

H&E staining (Fig. 7a) was applied to analyze the wound healing progress and histopathological changes. All of the wound beds had a certain degree of inflammatory response on the 7<sup>th</sup> day. This could be considered as an obvious inflammatory response as every wound passes through an essential inflammatory cycle. In particular, in comparison with the gauze group, the CDCE wound dressing had less inflammatory cell infiltration and more fibroblasts in the granulation tissue. On the 14<sup>th</sup> day, complete epidermis and blood vessels were formed in all groups. The statistical results of the granulation tissue thickness and epidermis thickness of the wounds covered by the various wound dressings are shown in Fig. 7c and d. The statistical results of the granulation tissue thickness of the wound dressing (Fig. 7c) indicated that the granulation tissue thickness of the wound treated by the CDCE wound dressing was significantly thicker than that of the gauze group. In particular, the CDCE-1 wound dressing could promote the growth of granulation tissue more than the CDA wound dressing or CDCE-2 wound dressing on the 7<sup>th</sup> day. Besides, the statistical results of the epidermis thickness of the wounds (Fig. 7d) treated with the CDCE wound dressing and the CDA

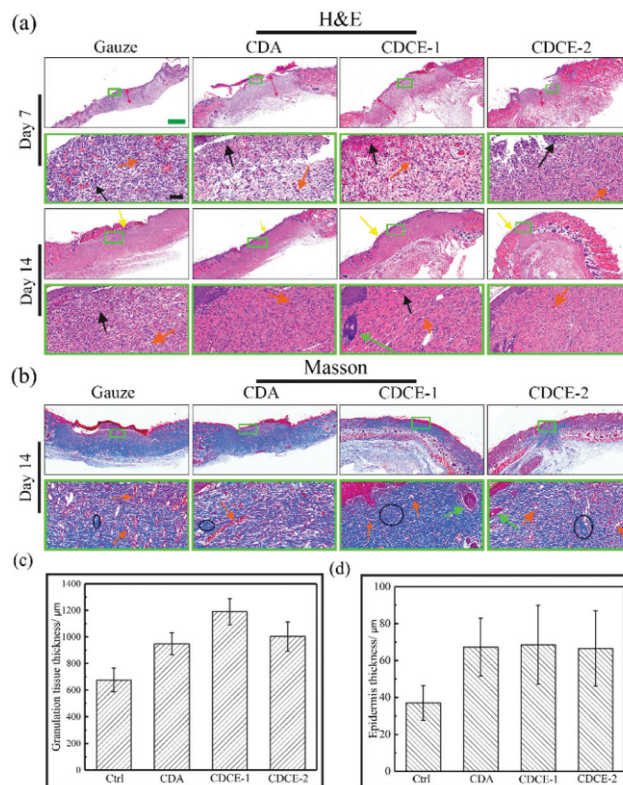


**Fig. 7** The histological analysis of wound regeneration tissues. (a) H&E staining and (b) Masson's trichrome staining of wound regeneration tissues treated with different wound dressings (green scale bar: 1 mm; black scale bar: 80 µm; red double-headed arrow: granulation tissue; black arrow: inflammation cells; pink arrow: blood vessels; yellow arrow: regenerated epithelialization; black circle: collagen fibers arrangement). (c) Granulation tissue thickness of wounds treated with different wound dressings on the 7<sup>th</sup> day. (d) Epidermis thickness of wounds treated with different wound dressings on the 14<sup>th</sup> day.

wound dressing were thicker than that in the gauze group, while there was no significant difference among the CDA and CDCE wound dressings on the 14<sup>th</sup> day. This may be due to the excellent antibacterial capacity and inhibition of an excessive wound inflammatory response, which could accelerate wound closure and promote damaged tissue regeneration.<sup>41,43,44</sup> Collagen deposition is a vital factor for the quality of the wound healing process.<sup>45</sup> Masson's trichrome staining was performed to evaluate collagen deposition in the newly formed tissues.<sup>41</sup> The results of the damaged tissues are shown in Fig. 7b. On the 14<sup>th</sup> day, the collagen bundles with the CDCE-1 wound dressing were denser. Moreover, the shape of the collagen was spindle, indicating the maturation of the collagen fiber, which indicated that the CDCE-1 wound dressing could significantly promote wound healing compared to the CDA wound dressing and gauze wound dressing. Additionally, the CDCE wound dressing could quickly eliminate the wound exudate, which could be of benefit to provide a suitable micro-environment.<sup>46</sup> In conclusion, the CDCE-1 wound dressing had antibacterial and anti-inflammatory properties, and the ability to quickly eliminate exudates, which

could promote early wound contraction and better quality of wound healing.<sup>4</sup>

### 3. Conclusions

In this work, a novel multifunctional cellulose diacetate-based composite wound dressing (CDCE) with rapid hemostasis, antibacterial properties, accelerated wound healing was successfully prepared. Due to its high water absorption, strong water absorbing capacity, high porosity and superhydrophilicity, the CDCE wound dressing could quickly eliminate wound exudate and further promote rapid hemostasis, which could provide a balanced moist micro-environment to promote wound healing. A wound dressing with rapid hemostasis could be of benefit to reduce mortality caused by excessive blood loss. In addition, excellent antibacterial properties could inhibit an excessive inflammatory response and accelerate wound healing. Thus, we believe that the multifunctional CDCE-1 wound dressing has high clinical application prospects in the future.

## 4. Experimental

### 4.1 Materials

Cellulose diacetate (CDA,  $M_w = 10^5 \text{ g mol}^{-1}$ ) was purchased from Aladdin Co. Ltd; 1,1,1,3,3,3-hexafluoro-2-propanol (HFIP) was purchased from Meryer Co. Ltd; carboxymethyl chitosan (CMC), tris(hydroxymethyl)aminomethane (Tris) and 3,4-dihydroxyphenyl thylamine hydrochloride (DA) were purchased from D&B Co. Ltd; poly(ethylene glycol) diglycidyl ether (PEGDE,  $M_n = 200 \text{ g mol}^{-1}$ ) and epsilon-poly-L-lysine ( $\epsilon$ -PL) were purchased from Macklin Co. Ltd; ethanol was purchased from Innochem Co. Ltd; 1-hydroxy-2,5-pyrrolidinedione (NHS)

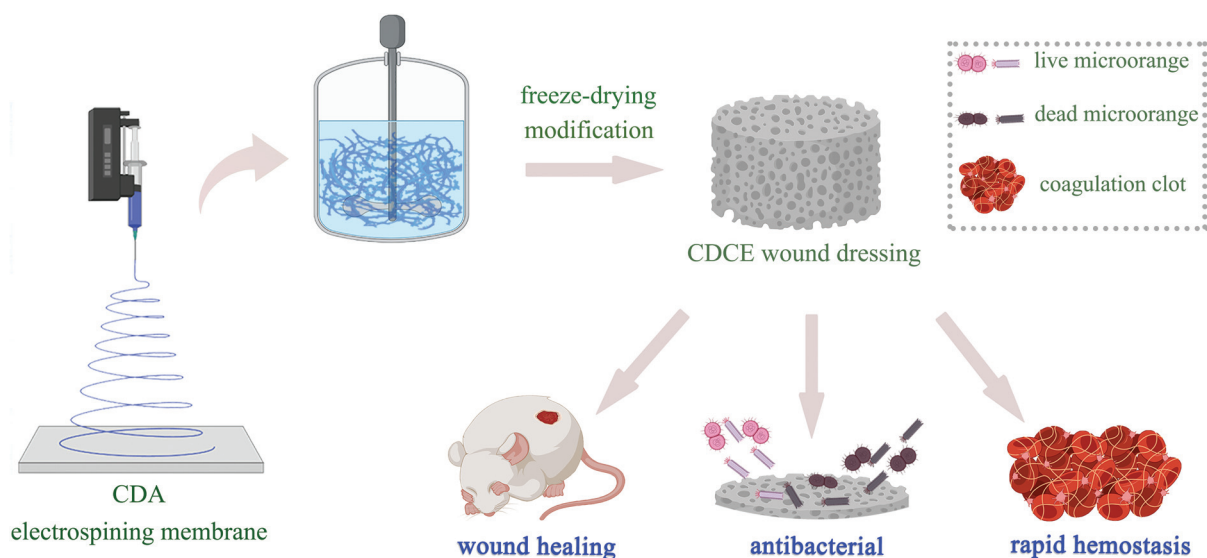
and 1-(3-dimethylamino propyl)-3-ethylcarbodiimide hydrochloride (EDC) were purchased from Titan Co. Ltd.

### 4.2 Preparation of the multifunctional CDCE wound dressing

The electrospinning of the CDA membrane was described in a previous report.<sup>47</sup> CDA (9 g) was dissolved in HFIP (100 g) under magnetic stirring to prepare the electrospinning precursor solution. The electrospinning of the nanofiber membrane was carried out by electrospinning equipment under 13 kV,  $2 \text{ ml h}^{-1}$  and 20 cm distance. The electrospun membrane was dried overnight to remove residual HFIP. Finally, short fibers were fabricated through homogenizer equipment (purchased from Joyang Co. Ltd) and dried in a vacuum oven.

To fabricate the cross-linked CDA wound dressing, 0.5 g short fibers were uniformly dispersed in a 25 g PEGDE aqueous solution ( $w_{\text{PEGDE}}:w_{\text{water}} = 1:99$ ). The homogeneous CDA short fiber suspension was transferred into a culture dish (diameter:9 cm) and frozen in a  $-20 \text{ }^\circ\text{C}$  refrigerator for 24 h, and then freeze-dried for 48 h to obtain a cross-linked CDA wound dressing. Finally, the wound dressings were transferred into  $70 \text{ }^\circ\text{C}$  DI water for dialysis for 48 h to remove residual PEGDE.

The antibacterial wound dressing was prepared through a post-modification strategy.<sup>48</sup> Briefly, the cross-linked CDA wound dressing was immersed into 100 ml of CMC Tris-HCl aqueous solution ( $\text{pH} = 8.5$ ). Subsequently, DA aqueous solution was dropped into the above aqueous solution and mechanically oscillated for 12 h. The as-prepared membrane (CDA@PDA/CMC) was purified with DI water for 24 h. Then, an amide reaction was carried out for 24 h between CDA@PDA/CMC and  $\epsilon$ -PL catalyzed by EDC/NHS. Finally, the antibacterial wound dressing was purified with DI water for 48 h and freeze-dried. A schematic illustration of the preparation of the multifunctional wound dressing is shown in Scheme 1. The composition of the wound dressings is presented in Table 1.



Scheme 1 Preparation of the multifunctional wound dressing.

**Table 1** Compositions of the multifunctional 3D wound dressings

	CDCE-1	CDCE-2	CDCE-3	CDCE-4
CMC g <sup>-1</sup>	0.4	0.4	0.4	0.4
DA g <sup>-1</sup>	0.2	0.2	0.2	0.2
ε-PL g <sup>-1</sup>	1.2	0.8	0.4	0.2

### 4.3 Wound dressing structure characterization

The structure of all samples was characterized by Fourier transform infrared (FT-IR, Nicolet 6700) through the KBr-pellet method, and the characterization range was 500–4000 cm<sup>-1</sup> with a resolution of 4 cm<sup>-1</sup>.

All samples were dried overnight in a vacuum oven before characterization, and coated with a gold layer. The morphology of the wound dressings was observed by scanning electron microscope (SEM: S-3400).

A moist wound micro-environment is important for cellular behavior, so the WVRT was determined by the gravimetric method.<sup>49</sup> Briefly, wound dressings (thickness: 0.3 ± 0.05 mm; diameter: 10 mm) were covered on the top of 5 ml glass test tubes. The glass test tubes were filled with 3 ml of DI water and placed in an oven at 37 °C for 24 h. The WVRT of the wound dressings was calculated according to the following formula.

$$\text{WVRT} = (w_0 - w_1)/AT \times 100\%$$

where  $w_0$  and  $w_1$  are the weight before and after the test, and  $A$  and  $T$  are the area of the wound dressing and 24 h.

The water absorbing rate was also determined by the gravimetric method.<sup>50</sup> Briefly, all samples were dried overnight in a vacuum oven before testing and weighed as  $w_0$ . Subsequently, the samples were immersed in saline solution and kept there for 10 s. Finally, the wet-wound dressing was removed from the saline solution and weighed as  $w_1$ . The water-absorbing rate was calculated through the following formula:

$$\text{water absorbing rate} = (w_1 - w_0)/w_0 \times 100\%$$

All samples were dried overnight in a vacuum oven and weighed as  $w_0$ , and then transferred into ethanol and kept there 30 s. Finally, the samples were removed from ethanol and weighed as  $w_1$ . The porosity of the wound dressings was calculated through the following formula:<sup>51</sup>

$$\text{porosity} = (w_1 - w_0)/\rho V_0 \times 100\%$$

Here,  $\rho$  and  $V_0$  are the corresponding density of ethanol and the volume of the dry wound dressing, respectively. The water contact angle was tested by a contact angle measurement system. All samples were evaluated 4 times and the mean value was calculated.<sup>52</sup>

### 4.4 *In vitro* antibacterial assay

An *in vitro* antibacterial assay was carried out through the colony-counting method.<sup>53,54</sup> Briefly, cylinder samples were sterilized by immersing them in 75% ethanol overnight and then immersed in a sterilized saline solution for 1 day under

UV-irradiation. Subsequently, the samples were co-cultured with bacterial suspension solution (*E. coli* or *S. aureus*) and co-cultured at 37 °C on a shaking table at 180 rpm for 4 h. Then, the bacterial suspension solution was diluted with saline solution and 20 μL was transferred to plate count agar and incubated at 37 °C for 20 h. The antibacterial rate was calculated through the following formula:

$$\text{antibacterial rate} = (n_0 - n_1)/n_0 \times 100\%$$

where  $n_0$  and  $n_1$  are the number of bacterial colonies on the control and test plate count agars, respectively.

To observe the bacterial morphology on the wound dressing surfaces and further study the antibacterial mechanism, all samples were co-cultured with bacterial suspension solution for 4 h. Subsequently, the bacteria were immobilized by 5 wt% glutaraldehyde aqueous solution and dehydrated by gradient ethanol. Finally, the bacterial morphology was observed by SEM.<sup>54</sup>

### 4.5 *In vitro* blood assay

The hemolysis rate of the wound dressing was determined by co-culturing with red blood cells (RBCs).<sup>38,51</sup> Briefly, all wound dressings were incubated in saline solution for 24 h at 37 °C beforehand, and then co-cultured with diluted RBC suspension solution ( $v_{\text{RBC}}:v_{\text{saline solution}} = 1:25$ ) for 1 h. Next, the co-cultured suspension solutions were centrifuged at 1500 rpm for 10 min to obtain the supernatants, and the absorbance was measured at 545 nm by a microplate reader (ELISA, BioTek). In addition, RBCs were co-cultured with DI water and saline solution as the negative control group and positive control group, respectively. The hemolysis ratio of the wound dressings was calculated according to the following formula:

$$\text{hemolysis rate} = (\text{OD}_s - \text{OD}_p)/(\text{OD}_n - \text{OD}_p) \times 100\%$$

where  $\text{OD}_s$ ,  $\text{OD}_p$  and  $\text{OD}_n$  are the absorbance of the supernatants of sample, positive and negative groups, respectively.

For the *in vitro* blood clotting index (BCI) assay, all wound dressings (diameter: 6 mm) were pre-warmed for 10 min, and then co-cultured with 100 μL of fresh anticoagulated rabbit blood containing CaCl<sub>2</sub> (10 μL, 0.1 M) for 10 min. Subsequently, 1 mL of DI water was added and the samples were incubated in a shaker for 5 min. The absorbance of the mixture solutions was measured at 545 nm by a microplate reader. In addition, a blank control was created by co-culturing 100 μL of fresh anticoagulated rabbit blood with 1 mL of DI water in a shaker for 5 min. The BCI of the wound dressings was calculated according to the following formula:

$$\text{BCI} = \text{OD}_s/\text{OD}_c \times 100\%$$

where  $\text{OD}_s$  and  $\text{OD}_c$  are the absorbance of the supernatants of the sample group and blank control, respectively.

For the RBC attachment assay, all wound dressings (diameter: 6 mm) were pre-warmed at 37 °C for 10 min, and then co-cultured with 100 μL of diluted RBC suspension solution for 1 min. Subsequently, unadhered RBCs were washed away with saline solution three times. The samples were then co-cul-

tured with 1 mL of DI water in a shaker for 5 min. In addition, a blank control was created by co-culturing 100  $\mu$ L of diluted RBC suspension solution with 1 mL of DI water in a shaker for 5 min. The absorbance of the mixture solution was measured at 545 nm by a microplate reader.

$$\text{RBC attachment rate} = \text{OD}_s / \text{OD}_c \times 100\%$$

where  $\text{OD}_s$  and  $\text{OD}_c$  are the absorbance of the supernatants of the sample groups and blank control, respectively.

The platelet (or RBC) morphology on the wound dressings was observed by SEM.<sup>38,55</sup> Briefly, all wound dressing were co-cultured with diluted platelet (or RBC) solution for 1 h, and then washed with saline solution to remove the unadhered platelets (or RBCs). Subsequently, the diluted platelet (or RBC) solution was stabilized by 5 wt% glutaraldehyde aqueous solution, dehydrated by gradient ethanol, and dried in a vacuum oven overnight.

#### 4.6 *In vivo* hemostasis assay

To investigate the hemostatic ability of the CDCE wound dressings *in vivo*, the research method was consistent with a previous report<sup>4</sup> and approved by the animal committee of Shanghai Tenth People's Hospital affiliated to Tongji University, China. Briefly, SD rats were successively anaesthetized and their livers exposed in an aseptic-environment. Then, the fluid around the liver was removed carefully by filter paper beforehand. Next, a bleeding liver wound model was made by surgical scissors. Subsequently, a cylinder wound dressing was covered on the liver wound. The blood loss of the liver was calculated by the gravimetric method. The blood from the liver was absorbed by pre-weighed filter paper, and then the filter paper was weighed again after absorbing blood. In addition, photos were taken to evaluate the hemostatic effects of the CDA and CDCE wound dressings.

#### 4.7 *In vitro* biocompatibility assay

In this work, the cell attachment rate of the wound dressings was determined by a low permeability crystal violet staining assay.<sup>50</sup> Briefly, all wound dressings were sterilized with 75% ethanol aqueous solution for 24 h under UV radiation and washed with saline solution for another 24 h. Next, mesenchymal stem cells (MSCs) were added at 50 000 cells per well and cultured in a 5%  $\text{CO}_2$  incubator at 37 °C for 4 h, 8 h and 12 h. Finally, the  $\alpha$ -MEM medium was removed and the cells were co-cultured with 500  $\mu$ L of crystal violet for 24 h. The cell numbers were then count under an optical microscope. The cell attachment rate of the wound dressings was calculated according to the following formula:

$$\text{cell attachment rate} = n_1 / 50\,000 \times 100\%$$

where  $n_1$  is the number of cells attached on the wound dressing surface at different time points.

The cytocompatibility of the wound dressings was evaluated by a cell counting kit-8 (CCK-8, Yeasen) assay.<sup>56,57</sup> Briefly, the wound dressings were sterilized with 75% ethanol aqueous solution for 24 h and incubated with  $\alpha$ -MEM medium for

another 24 h at 37 °C beforehand. Next, the wound dressings were transferred into 48-well cell culture plates and MSCs were added at 5000 cells per well, then cultured in a 5%  $\text{CO}_2$  incubator at 37 °C. The  $\alpha$ -MEM medium was changed every 3 days. After culturing for 2 days, 4 days and 6 days, the absorbance was evaluated at 450 nm by a microplate reader after staining by CCK-8. The cell viability of the CDA wound dressing was set as 100%. The cell viability of the wound dressings was calculated according to the following formula:

$$\text{cell viability} = \text{OD}_1 / \text{OD}_0 \times 100\%$$

where  $\text{OD}_0$  and  $\text{OD}_1$  are the absorbance of the CDA wound dressing and CDCE wound dressing co-cultured with MSCs, respectively.

To observe the MSC morphology on the wound dressings, the wound dressings were co-cultured with MSCs at 50 000 cells per well for 6 days, and then fixed with 5 wt% glutaraldehyde aqueous solution overnight. Next, the wound dressings were washed with saline solution and dehydrated by gradient ethanol solution, then dried in a vacuum oven overnight. The MSC morphology was observed by SEM.

Living/dead staining of cells was performed using calcein-AM/propidium iodide.<sup>56</sup> Briefly, the wound dressings were co-cultured with MSCs at 50 000 cells per well for 6 days, and then stained by calcein-AM/propidium iodide solution. The images of the cells stained by fluorochrome staining were obtained by laser confocal microscopy (LEICA, TCS, SP8).

#### 4.8 *In vivo* evaluation of wound healing

The *in vivo* wound healing assay was performed according to previous reports and approved by the animal committee of Shanghai Tenth People's Hospital affiliated to Tongji University, China.<sup>22,51,58</sup> Briefly, firstly, all SD rats (6–8 weeks, 250–300 g) were anaesthetized with chloral hydrate. Next, four circular full-thickness skin wounds with 1.5 cm diameter were created on the dorsal area of each SD rat. Subsequently, all full-thickness wounds were covered by gauze, CDA wound dressing, CDCE wound dressing, respectively. And then all wound dressings were stabled by circular metal model on the wounds surface to ensure that the wound dressing could fit with the wound. Gauze, a common traditional wound dressing, was the control group in this work. The wound area tissues were collected on the 7<sup>th</sup> day and 14<sup>th</sup> day. To evaluate the wound healing on the 7<sup>th</sup> day and 14<sup>th</sup> day, the wound tissue thickness slices were stained by Haematoxylin-Eosin (H&E, Beyotime, China) and Masson's trichrome (Beyotime). All photographs were taken by an inverted fluorescence microscope (Nikon ECLIPSE Ti-S).

## Ethical statement

All animal procedures were performed in accordance with the Guidelines for Care and Use of Laboratory Animals of Tongji University and approved by the Animal Ethics Committee of Shanghai tenth people's hospital affiliated to Tongji University.

## Author contributions

W. C. Liang, J. Li and M. D. Lang designed the research and finished the paper; Q. H. Lu, F. Yu, J. Y. Zhang, and C. Xiao helped performed the research; J. Li helped with the *in vivo* assay; D. X. Dou, Y. Zhou, X. M. Mo and M. D. Lang helped revise the paper.

## Conflicts of interest

There are no conflicts to declare.

## Acknowledgements

This research was supported by the National Key Research and Development Program (2016YFC1100703). The authors thank Research Center of Analysis and Test of East China University of Science and Technology for the help with the characterization.

## References

- 1 Y. P. Liang, X. Zhao, T. L. Hu, B. J. Chen, Z. H. Yin, P. X. Ma and B. L. Guo, *Small*, 2019, **15**, e1900046.
- 2 H. Hu and F. J. Xu, *Biomater. Sci.*, 2020, **8**, 2084–2101.
- 3 X. Zhao, B. L. Guo, H. Wu, Y. P. Liang and P. X. Ma, *Nat. Commun.*, 2018, **9**, 2784.
- 4 L. I. Gao, J. J. Chen, W. Feng, Q. Song, J. J. Huo, L. F. Yu, N. Liu, T. J. Wang, P. Li and W. Huang, *Biomater. Sci.*, 2020, **8**, 6930–6945.
- 5 J. H. He, Y. P. Liang, M. T. Shi and B. L. Guo, *Chem. Eng. J.*, 2020, **385**, 123464.
- 6 M. L. Yin, S. S. Wan, X. h. Ren and C.-C. Chu, *ACS Appl. Mater. Interfaces*, 2021, **12**, 14688–14699.
- 7 B. Dalisson and J. Barralet, *Adv. Healthcare Mater.*, 2019, **8**, e1900764.
- 8 K. Wang, J. W. L. Li, L. Q. Xu, N. Feng, Y. Wang, X. Fei, J. Tian and Y. Li, *Chem. Eng. J.*, 2019, **372**, 216–225.
- 9 H. J. Zhang, M. X. Peng, G. Z. Lu, T. Cheng, P. Zhao, L. P. Qiu, J. Zhou and J. H. Chen, *J. Mater. Sci.*, 2018, **53**, 14944–14952.
- 10 B. B. Xu, Y. J. Liu, X. W. Sun, J. H. Hu, P. Shi and X. Y. Huang, *ACS Appl. Mater. Interfaces*, 2017, **19**, 16517–16523.
- 11 J. Zhang, R. T. Zhou, H. Wang, X. Y. Jiang, H. Y. Wang, S. J. Yan, J. H. Yin and S. F. Luan, *Appl. Surf. Sci.*, 2019, **497**, 143480.
- 12 A. C. Strömdahl, L. Ignatowicz, G. Petruka, M. Butrym, S. Wasserstrom, A. Schmidtchen and M. Puth, *Acta Biomater.*, 2021, **128**, 314–331.
- 13 C. C. Zhou, P. Li, X. B. Qi, A. R. Mohamed Sharif, Y. F. Poon, Y. Cao and M. W. Chang, *Biomaterials*, 2011, **32**, 2704–2712.
- 14 R. Wang, J. Z. Li, W. Chen, T. T. Xu, S. F. Yun, Z. Xu, Z. Q. Xu, T. Sato, B. Chi and H. Xu, *Adv. Funct. Mater.*, 2017, **27**, 1604894.
- 15 A. Tchobanian, H. Van Oosterwyck and P. Fardim, *Carbohydr. Polym.*, 2019, **205**, 601–625.
- 16 Y. Wang, L. N. Zhang and A. Lu, *ACS Appl. Mater. Interfaces*, 2019, **44**, 41710–41716.
- 17 N. Li, L. Q. Yang, C. L. Pan, P. Er Saw, M. Ren, B. Y. Lan, J. F. Wu, X. Y. Wang, T. T. Zeng, L. Y. Zhou, L. M. Zhang, C. Yang and L. Yan, *Acta Biomater.*, 2020, **102**, 298–314.
- 18 W. C. Liang, J. Huo, X. C. Fang, F. D. Bai, T. H. Zhu, F. F. Gao, C. Wei, X. M. Mo and M. D. Lang, *Appl. Surf. Sci.*, 2018, **443**, 374–381.
- 19 H. X. Li, T. Wu, J. J. Xue, Q. F. Ke and Y. N. Xia, *Macromol. Rapid Commun.*, 2020, **41**, e1900579.
- 20 K. k. Wu, X. X. Wu, J. S. Guo, Y. P. Jiao and C. G. Zhou, *Adv. Healthcare Mater.*, 2021, e2100793.
- 21 W. M. Chen, S. Chen, Y. Morsi, H. El-Hamshary, M. El-Newhy, C. Y. Fan and X. M. Mo, *ACS Appl. Mater. Interfaces*, 2016, **8**, 24415–24425.
- 22 J. Li, F. Yu, G. Chen, J. Liu, X. L. Li, B. Cheng, X. M. Mo, C. Chen and J. F. Pan, *ACS Appl. Mater. Interfaces*, 2020, **12**, 2023–2038.
- 23 C. Feng and X. Y. Huang, *Acc. Chem. Res.*, 2018, **9**, 2314–2323.
- 24 X. M. Bao, X. R. Fan, Y. Y. Yu, Q. Wang, P. Wang and J. G. Yuan, *Int. J. Biol. Macromol.*, 2020, **144**, 267–278.
- 25 A. S. Montaser, M. Rehan, W. M. El-Senousy and S. Zaghoul, *Carbohydr. Polym.*, 2020, **244**, 116479.
- 26 Q. B. Xu, W. S. Zheng, P. P. Duan, J. N. Chen, Y. Y. Zhang, F. Y. Fu, H. Y. Diao and X. D. Liu, *Carbohydr. Polym.*, 2019, **204**, 42–49.
- 27 Q. B. Xu, W. S. Zheng, P. P. Duan, J. N. Chen, Y. Y. Zhang, F. Y. Fu, H. Y. Diao and X. D. Liu, *Carbohydr. Polym.*, 2019, **204**, 42–49.
- 28 H. Zhang, C. W. Chen, H. Zhang, G. P. Chen, Y. T. Wang and Y. J. Zhao, *Appl. Mater. Today*, 2021, **23**, 101068.
- 29 Y. Shen, L. L. Wang, F. Liu, H. Z. Liu, D. W. Li, Q. S. Liu and B. Y. Deng, *ACS Appl. Mater. Interfaces*, 2020, **12**, 53104–53114.
- 30 J. Xia, H. Zhang, F. Q. Yu, Y. Pei and X. G. Luo, *ACS Appl. Mater. Interfaces*, 2020, **21**, 24370–24379.
- 31 Z. W. Qiao, X. L. Lv, S. H. He, S. M. Bai, X. C. Liu, L. X. Hou, J. J. He, D. M. Tong, R. J. Ruan, J. Zhang, J. X. Ding and H. H. Yang, *Bioact. Mater.*, 2021, **9**, 2829–2840.
- 32 H. Cheng, Z. Shi, K. Yue, X. S. Huang, Y. C. Xu, C. H. Gao, Z. Q. Yao, Yu S. Zhang and J. Wang, *Acta Biomater.*, 2021, **124**, 219–232.
- 33 X. Ke, Z. Y. Dong, S. X. Tang, W. L. Chu, X. R. Zheng, L. Zhen, X. Y. Chen, C. M. Ding and J. S. Li, *Biomater. Sci.*, 2020, **8**, 4346–4357.
- 34 X. L. He, Y. P. Yang, H. D. Song, S. Wang, H. Zhao and D. S. Wei, *ACS Appl. Mater. Interfaces*, 2020, **12**, 14784–14796.
- 35 D. A. Hickman, C. L. Pawlowski, U. D. S. Sekhon, J. Marks and A. SenGupta, *Adv. Mater.*, 2018, **30**, 10.
- 36 Z. Ahmadian, A. Correia, M. Hasany, P. Figueiredo, F. Dobakhti, M. R. Eskandari, S. H. Hosseini, R. Abiri,

- S. Khorshid, J. Hirvonen, H. A. Santos and M.-A. Shahbazi, *Adv. Healthcare Mater.*, 2020, **10**, e2001122.
- 37 L. Y. Wang, X. R. You, C. L. Dai, T. Tong and J. Wu, *Biomater. Sci.*, 2020, **8**, 4396–4412.
- 38 W. W. Qiu, H. Han, M. N. Li, N. Li, Q. Wang, X. H. Qin, X. L. Wang, J. Y. Yu, Y. X. Zhou, Y. Li, F. X. Li and D. Q. Wu, *J. Colloid Interface Sci.*, 2021, **596**, 312–323.
- 39 A. Tang, Y. Li, Y. Q. Yao, X. X. Yang, Z. J. Cao, H. L. Nie and G. Yang, *Biomater. Sci.*, 2021, **9**, 4169–4177.
- 40 S. Chen, W. M. Chen, Y. N. Chen, X. M. Mo and C. Y. Fan, *Mater. Sci. Eng. Carbon*, 2021, **118**, 111312.
- 41 Z. F. Yang, R. K. Huang, B. N. Zheng, W. T. Guo, C. K. Li, W. Y. He, Y. Q. Wei, Y. Du, H. M. Wang, D. C. Wu and H. Wang, *Adv. Sci.*, 2021, **8**, 2003627.
- 42 L. N. Fu, J. Zhang and G. Yang, *Carbohydr. Polym.*, 2013, **92**, 1432–1442.
- 43 T. Xia, F. Xie, X. E. Bian, Z. H. Chen, S. C. Zhang, Z. H. Fang, Q. F. Ye, J. Cai and Y. F. Wang, *Mater. Sci. Eng. Carbon*, 2021, **126**, 112177.
- 44 Z. J. Xu, B. Liang, J. Z. Tian and J. Wu, *Biomater. Sci.*, 2021, **9**, 4388–4409.
- 45 K. X. Zhang, X. Y. Jiao, L. P. Zhou, J. Wang, C. Wang, Y. Qin and Y. Q. Wen, *Biomaterials*, 2021, **276**, 121040.
- 46 D. Y. Chen, X. Y. Zhou, L. M. Chang, Y. Wang, W. J. Li and J. L. Qin, *Biomacromolecules*, 2021, **22**, 2272–2283.
- 47 J. Fang, S. H. Ye, J. Wang, T. Zhao, X. M. Mo and W. R. Wagner, *Biomacromolecules*, 2015, **16**, 1622–1633.
- 48 Y. Lv, H. C. Yang, H. Q. Liang, L. S. Wan and Z. K. Xu, *J. Membr. Sci.*, 2015, **476**, 50–58.
- 49 S. Fahimirad, H. Abtahi, P. Satei, E. Ghaznavi-Rad, M. Moslehi and A. Ganji, *Carbohydr. Polym.*, 2021, **259**, 117640.
- 50 W. C. Liang, M. L. Jiang, J. Y. Zhang, X. M. Dou, Y. Zhou, Y. Jiang, L. Zhao and M. D. Lang, *J. Mater. Sci. Technol.*, 2020, **89**, 225–232.
- 51 M. P. Tian, A. D. Zhang, Y. X. Yao, X. G. Chen and Y. Liu, *Carbohydr. Polym.*, 2021, **261**, 117878.
- 52 B. B. Xu, C. Feng, J. H. Hu, P. Shi, G. X. Gu, L. Wang and X. Y. Huang, *ACS Appl. Mater. Interfaces*, 2016, **10**, 6685–6692.
- 53 Z. W. Liu, X. Y. Zhao, B. R. Yu, N. N. Zhao, C. Zhang and F. J. Xu, *ACS Nano*, 2021, **15**, 7482–7490.
- 54 W. C. Huang, R. Ying, W. Wang, Y. N. Guo, Y. J. He, X. Y. Mo, C. H. Xue and X. Z. Mao, *Adv. Funct. Mater.*, 2020, **30**, 1.
- 55 X. Yang, W. Liu, G. H. Xi, M. S. Wang, B. Liang, Y. F. Shi, Y. K. Feng, X. K. Ren and C. C. Shi, *Carbohydr. Polym.*, 2019, **222**, 115012.
- 56 Y. J. Zhong, F. Seidi, C. C. Li, Z. M. Wan, Y. C. Jin, J. L. Song and H. N. Xiao, *Biomacromolecules*, 2021, **22**, 1654–1663.
- 57 C. Zhang, Y. S. Zhou, H. J. Han, H. X. Zheng, W. H. Xu and Z. K. Wang, *ACS Nano*, 2021, **15**, 1785–1794.
- 58 J. Qu, X. Zhao, Y. P. Liang, Y. M. Xu, P. X. Ma and B. L. Guo, *Chem. Eng. J.*, 2019, **362**, 548–560.